Original Article

Use of biexponential and stretched exponential models of intravoxel incoherent motion and dynamic contrast-enhanced magnetic resonance imaging to assess the proliferation of endometrial carcinoma

Gaiyun Zhang[1#], Ruifang Yan[1#], Wangyi Liu[1#], Xingxing Jin[1#], Xuejia Wang[1], Hongxia Wang[1], Zhong Li[1], Jie Shang[2], Kaiyu Wang[3], Jinxia Guo[3], Dongming Han[1]

[1]Department of Magnetic Resonance, The First Affiliated Hospital, Xinxiang Medical University, Weihui, China; [2]Department of Pathology, The First Affiliated Hospital, Xinxiang Medical University, Weihui, China; [3]Magnetic Resonance Research China, GE Healthcare, Beijing, China

Contributions: (I) Conception and design: D Han, R Yan; (II) Administrative support: D Han, R Yan; (III) Provision of study materials or patients: G Zhang, W Liu, X Wang, H Wang; (IV) Collection and assembly of data: X Jin, Z Li, W Liu, X Wang, H Wang; (V) Data analysis and interpretation: J Guo, K Wang, J Shang; (VI) Manuscript writing: All authors; (VII) Final approval of manuscript: All authors.

[#]These authors contributed equally to this work and should be considered as co-first authors.

Correspondence to: Dongming Han. Department of Magnetic Resonance, The First Affiliated Hospital, Xinxiang Medical University, 88 Jiankang Road, Weihui 453100, China. Email: 625492590@qq.com.

Background: It is important to assess the proliferation of endometrial carcinoma (EC) noninvasively using imaging methods. This prospective diagnostic study investigated the value of biexponential and stretched exponential models of intravoxel incoherent motion (IVIM) and dynamic contrast-enhanced magnetic resonance imaging (DCE-MRI) in predicting the Ki-67 status of EC.

Methods: In all, 70 patients with EC underwent pelvic MRI. The diffusion coefficient (D), pseudo diffusion coefficient (D*), perfusion fraction (f), distributed diffusion coefficient (DDC), water molecular diffusion heterogeneity index (α), volume transfer constant (K^{trans}), rate transfer constant (K_{ep}), and volume of extravascular extracellular space per unit volume of tissue (V_e) were compared. The area under the receiver operating characteristic (ROC) curve (AUC) was used to quantify diagnostic efficacy. Multivariate logistic regression and bootstrap (1,000 samples) analyses were used to establish and evaluate, respectively, the optimal model to predict Ki-67 status.

Results: D, K^{trans}, and K_{ep} were lower while α was higher in the high-proliferation group as compared with low-proliferation group (all P values<0.05). D and K_{ep} were independent predictors of Ki-67 status in EC, and the combination of these parameters had optimal diagnostic efficacy (AUC =0.920; sensitivity 85.71%; specificity 89.29%), which was significantly better than that of D (AUC =0.753; Z=2.874; P=0.004), α (AUC =0.715; Z=3.505; P=0.001), K^{trans} (AUC =0.808; Z=2.741; P=0.006), and K_{ep} (AUC =0.832; Z=2.147; P=0.032) alone. The validation model showed good accuracy (AUC =0.882; 95% confidence interval 0.861–0.897) and consistency (C-statistic =0.902). D, K_{ep}, K^{trans}, and α showed a slightly negative (r=–0.271), moderately negative (r=–0.534), slightly negative (r=–0.409), and slightly positive (r=0.488) correlation with the Ki-67 index, respectively (all P values <0.05).

Conclusions: IVIM- and DCE-MRI-derived parameters, including D, α, K^{trans}, and K_{ep}, were associated with Ki-67 status in EC, and the combination of D and K_{ep} may serve as a superior imaging marker for the identification of low- and high-proliferation EC.

Keywords: Dynamic contrast-enhanced magnetic resonance imaging (DCE-MRI); endometrial carcinoma (EC); intravoxel incoherent motion (IVIM); proliferation status

Submitted Jun 28, 2022. Accepted for publication Jan 20, 2023. Published online Feb 16, 2023.
doi: 10.21037/qims-22-688
View this article at: https://dx.doi.org/10.21037/qims-22-688

Introduction

Endometrial carcinoma (EC) is a common malignant tumor of the female reproductive organs, and the disorderly proliferation of tumor cells is one of the key contributors to its lethality (1). Ki-67 is a nuclear protein that reflects abnormal cell proliferation, and previous studies have shown that EC with higher Ki-67 expression tends to be more aggressive and have a worse prognosis (2,3). Therefore, the accurate assessment of the Ki-67 expression levels in relevant lesions before treatment will improve the diagnosis and prognostic assessment of patients with EC. Currently, biopsy is the primary means to obtaining preoperative information regarding Ki-67 in EC. However, due to drawbacks such as susceptibility to operator experience, inadequate sampling, and invasiveness, biopsy may not be sufficient to obtain reliable results (4,5).

In clinical practice, magnetic resonance imaging (MRI) is an important tool for providing diagnostic information to guide EC patient management (6). However, conventional MRI sequences can only assess the macroscopic morphological features of lesions, which makes it challenging to effectively evaluate features involving cellular microscopic information, such as Ki-67. Compared with conventional MRI, quantitative MRI can accurately assess the microscopic information of tissues, and with the continued progress in related technologies, an increasing number of studies have emphasized the growing contribution of quantitative MRI as a source of quantitative biomarkers (7,8). Intravoxel incoherent motion (IVIM) is a promising quantitative MRI sequence in which the biexponential model can reflect the true diffusion information and microcirculatory perfusion of water molecules in tissues, whereas the stretched exponential model describes the average diffusion information of water molecules and structural complexity in tissues (9,10). Dynamic contrast-enhanced MRI (DCE-MRI) is another quantitative MRI imaging sequence that mainly analyzes the dynamic distribution of contrast agents through the pharmacokinetic model to quantitatively detect the blood supply of biological tissues (11). Numerous studies have demonstrated the usefulness of IVIM and DCE-MRI in the diagnosis and evaluation of diseases such as head and neck, breast, and abdominopelvic disorders (12-16). Meanwhile, IVIM and DCE-MRI have been used in some EC-related studies. For example, Meng *et al.* and Ye *et al.* used IVIM and DCE-MRI, respectively, for the preoperative risk assessment of EC and found that some of the parameters of IVIM and DCE-MRI were helpful in differentiating between EC risk groups (17,18). Satta *et al.* used both the biexponential model IVIM and DCE-MRI to assess the grade, stage, and other histopathological features of EC and showed that some of the derived parameters had a positive effect on the assessment of the histopathological features of EC (19).

However, to the best of our knowledge, no studies that have used biexponential model IVIM and stretched exponential model IVIM, and DCE-MRI to assess EC in the same population. The purpose of this study was to explore the value of biexponential model IVIM, stretched exponential model IVIM, and DCE-MRI in the prediction of the Ki-67 status in patients with EC, with the aim of providing a reliable imaging marker for the differentiation of EC into high- and low-proliferation groups. We present the following article in accordance with the STARD reporting checklist (available at https://qims.amegroups.com/article/view/10.21037/qims-22-688/rc).

Methods

Study patients

The study was conducted in accordance with the Declaration of Helsinki (as revised in 2013). This prospective study complied with ethical committee standards and was approved by the Ethics Committee of the First Affiliated Hospital of Xinxiang Medical University (No. EC-022-002). All participants provided informed consent. Between March 2021 and May 2022, 100 female patients with a first diagnosis of suspected EC at our institution underwent pelvic MRI. Of these 100 patients, 30 were excluded because of histologically proven non-EC (n=10), incomplete scan sequences or poor image quality in IVIM or DCE-MRI sequences (n=8), previous radiotherapy or neoadjuvant chemotherapy (n=7), and the absence of histopathological or immunohistochemical

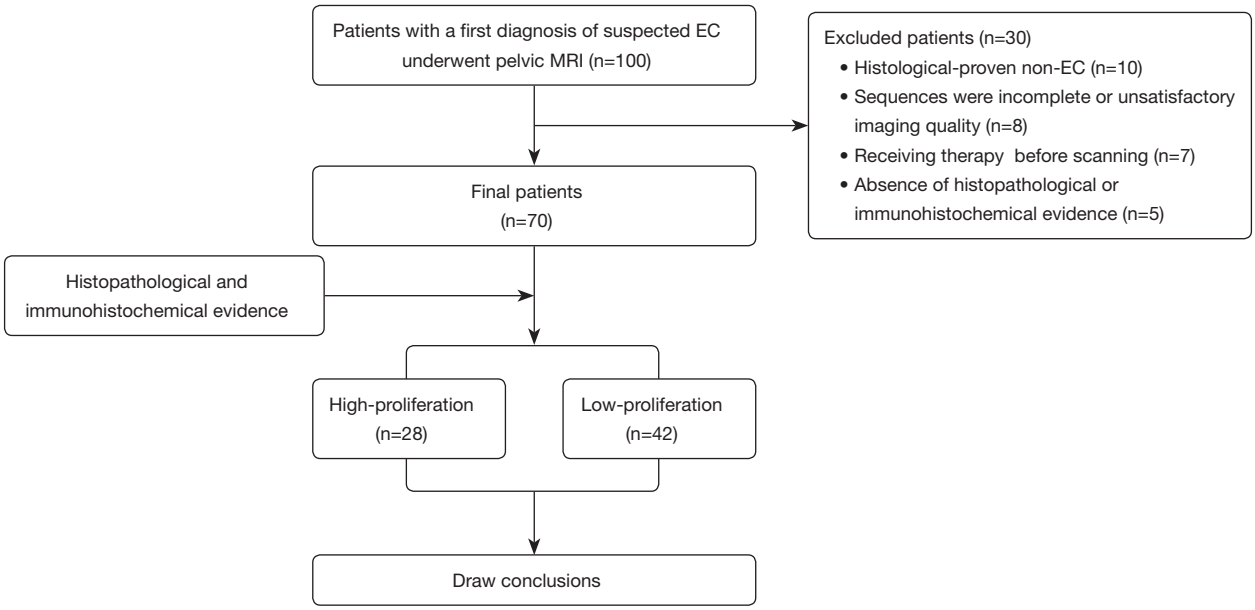

Figure 1 Study flowchart. EC, endometrial carcinoma; MRI, magnetic resonance imaging.

evidence (n=5; *Figure 1*).

MRI protocols

Scans were performed using a 1.5-T magnetic resonance (MR) system (Optima MR360; GE Healthcare, Chicago, IL, USA) with a 12-channel phased-array body coil. The scanning protocol included oblique axial T_1-weighted imaging (T_1WI), T_2-weighted imaging (T_2WI), diffusion-weighted imaging (DWI), IVIM, and DCE-MRI. For T_1WI, T_2WI, DWI, and DCE-MRI, the scans covered the anterior superior iliac spine to the symphysis pubis. For IVIM (b=0, 20, 40, 80, 160, 200, 400, 600, 800, and 1,000 s/mm^2), to minimize scan time, the scan range was limited to the tumor area (identified by an experienced radiologist from the DWI images), and the location, layer thickness, and layer spacing were consistent with the corresponding layer on DWI. The DCE-MRI images were obtained using a 3-dimensional liver acquisition with volume acceleration (3D-LAVA) sequence with a temporal resolution of 9 s. Sequential images were acquired from 9 s before intravenous injection of gadopentetate diethylenetriaminepentaacetic acid (Gd-DTPA; 0.2 mL/kg, 3.0 mL/s; Bayer Pharmaceutical, Berlin, Germany) to 360 s after. The protocol details are provided in *Table 1*.

Image post-processing

All images were transferred to the Advantage Workstation (version 4.7; GE Healthcare). GenIQ software based on a Tofts model within the workstation was used for DCE-MRI analysis, and the arterial input function (AIF) was obtained from the internal iliac artery. The rate transfer constant, K_{ep}, represents the diffusion of contrast medium from the extravascular extracellular space (EES) to the vessel and is calculated using the volume transfer constant, K^{trans}, which indicates the diffusion of contrast medium from the vessel to the EES and the volume of EES per unit volume of tissue (V_e), as reported by Khalifa *et al.* (11):

$$K_{ep} = K^{trans} / V_e \quad [1]$$

MADC software within the workstation was used for IVIM analysis. The parameters of the biexponential model IVIM were calculated using the following formula:

$$S_b / S_0 = (1-f) \times \exp(-bD) + f \times \exp\left[-b \times (D^*)\right] \quad [2]$$

where S_0 is signal intensity at b=0, S_b is signal intensity at the b value denoted by the subscript, D is the true diffusion coefficient, f is the perfusion fraction, and D^* is the pseudo diffusion coefficient (9). The parameters of the stretched exponential model IVIM were derived using the following equation functions:

Table 1 Imaging protocol parameters

Parameter	T_1WI	T_2WI	DWI	IVIM	DCE-MRI
Sequence	2D FSE	2D FSE	2D SS-EPI	2D SS-EPI	3D LAVA
Orientation	Oblique axial	Oblique axial	Oblique axial	Oblique axial	Oblique axial
TR/TE (ms)	659/12.3	6,000/95	3,708/74.3	2,000/80.7	3.5/1.7
FOV (cm^2)	40×40	40×40	40×40	40×40	36×36
Matrix	288×192	320×320	96×128	128×192	288×192
Flip angle (°)	160	160	90	90	15
Slice thickness (mm)	6	6	6	6	6
No. sections	20	20	20	Based on lesion size	26
No. excitations	1	1	1, 4	1, 1, 1, 1, 1, 1, 2, 4, 4, 6	0.73
Fat suppression	–	STIR	STIR	STIR	FLEX
b values (s/mm^2)	–	–	0, 800	0, 20, 40, 80, 160, 200, 400, 600, 800, 1,000	–
Respiratory compensation	Free	Free	Free	Free	Free
Scan time	1 min 56 s	48 s	1 min 04 s	3–6 min	6 min 08 s (40 phases)

TR/TE, repetition time/echo time; FOV, field of view; T_1WI, T_1-weighted imaging; T_2WI, T_2-weighted imaging; DWI, diffusion-weighted imaging; IVIM, intravoxel incoherent motion; DCE-MRI, dynamic contrast-enhanced magnetic resonance imaging; 2D, 2-dimensional; FSE, fast spin echo; SS-EPI, single-shot echo planar imaging; 3D, 3-dimensional; LAVA, liver acquisition with volume assessment; STIR, short inversion time recovery; FLEX, flexible.

$$S_b / S_0 = \exp\left[-(b \times DDC)^{\alpha}\right] \quad [3]$$

where *DDC* is the distributed diffusion coefficient and α is the water molecular diffusion heterogeneity index (10). On IVIM images with a b value of 800 s/mm^2, 2-dimensional (2D) regions of interest (ROIs) were delineated layer by layer for all layers containing the tumor, and these 2D ROIs were manually drawn along the inside margin of the primary tumor, avoiding areas with cystic degeneration, necrosis, apparent signs and hemorrhage artifacts, and blood vessels. Subsequently, all completed 2D ROIs were automatically copied to the pseudo color maps of IVIM-derived parameters to calculate the parameter values, and the final parameter value for each tumor was the average of the corresponding parameter on all slices (17). For DCE-MRI, among the 40 phases scanned, the images of the phase with the clearest lesion display were selected to delineate the 2D ROIs, and the specific method was the same as that used for IVIM. Two radiologists (GYZ and RFY, with 6 and 20 years experience, respectively), without knowledge of the clinical and pathological information and each other's outcomes, delineated the ROIs and generated the corresponding parameter values, respectively.

Histopathologic and Ki-67 expression analyses

All lesion specimens were obtained surgically, and the median interval from pelvic MRI examination to surgery was 12 days (range, 1–25 days). Hematoxylin and eosin (HE) staining was used to determine histological type. A murine Ki-67 monoclonal antibody (M3G4; Celnovte Biotechnology, Zhengzhou, China) was used to determine the Ki-67 index. Five hotspots (areas with a high number of Ki-67-positive cells) were selected at a magnification of 400×; in each hotspot, 100 tumor cells were evaluated, with the proportion of positive cells used as an indicator of Ki-67 expression. Patients were divided into two proliferation groups based on Ki-67 expression: the low-proliferation group was defined as having slightly positive (+; <10%) and positive (++; 10–50%) Ki-67 expression, whereas the high-proliferation group was defined as having strongly positive (+++; >50%) Ki-67 expression.

Statistical analysis

MedCalc version 15.0 (MedCalc Software, Ostend, Belgium) and Stata version 16.0 (StataCorp., College

Station, TX, USA) were used for data analysis. The interobserver agreement of parameter measurements was evaluated by intraclass correlation coefficients (ICCs); ICC <0.4, 0.41–0.60, 0.60–0.75, and >0.75 indicated positive but poor, fair, good, and excellent agreement, respectively (20). The Shapiro-Wilk test was used to check the normality of the data. Data that were not normally distributed are presented as the median and interquartile range (IQR), with differences between the Ki-67 high-proliferation and low-proliferation groups evaluated using the Mann-Whitney test. Normally distributed data are presented as the mean ± SD and were compared between groups using the independent samples *t* test. The area under the receiver operating characteristic (ROC) curve (AUC) was used to quantify diagnostic efficacy, and differences were assessed using DeLong analysis. The combination model for predicting the Ki-67 status of EC was investigated by using multivariate logistic regression and evaluated by bootstrap (1,000 samples), ROC curves, calibration curves, and decision curve analysis (DCA) (21). The correlation between each parameter and Ki-67 was described by Spearman rank correlation, with $|r|$<0.25, 0.25–0.50, 0.50–0.75, and >0.75 indicating positive but little, mild, moderate, and good correlation, respectively.

Results

Patient information

In all, 70 patients were enrolled in the study. Imaging characteristics are shown in *Figure 2* and clinicopathological characteristics are summarized in *Table 2*.

Interobserver consistency

There was excellent consistency in D, D*, f, DDC, α, K^{trans}, V_e, and K_{ep} as measured by the 2 radiologists, with ICCs of 0.888 [95% confidence interval (CI): 0.795–0.935], 0.814 (95% CI: 0.711–0.881), 0.841 (95% CI: 0.75–0.898), 0.868 (95% CI: 0.795–0.916), 0.851 (95% CI: 0.771–0.905), 0.885 (95% CI: 0.822–0.927), 0.854 (95% CI: 0.776–0.907), and 0.844 (95% CI: 0.761–0.900), respectively. Averaged results were used for the final analysis.

Parameter comparison

D, K^{trans}, and K_{ep} were significantly lower (all P values <0.001), and α was significantly higher (P=0.001), in the high-proliferation group than in the low-proliferation group. There was no statistically significant difference in D*, f, DDC, and V_e between the two groups (P=0.206, P=0.590, P=0.136, and P=0.124, respectively; *Table 3*).

Regression analyses

Potential predictive factors, such as age, tumor size, International Federation of Gynecology and Obstetrics (FIGO) stage, D, D*, f, DDC, α, K^{trans}, V_e, and K_{ep}, were investigated with logistic regression analysis to evaluate their ability to identify high-proliferation and low-proliferation EC. Univariate analysis demonstrated that age, FIGO stage, D, α, K^{trans}, and K_{ep} were all predictors of EC proliferation (P=0.014, P=0.042, P=0.002, P=0.004, P=0.001, and P=0.001, respectively), whereas multivariate analysis showed that only D (P=0.013) and K_{ep} (P=0.031) were independent predictors (*Table 4*).

Diagnostic performance

In the differentiation of high-proliferation and low-proliferation EC, the combination of the independent predictors (D and K_{ep}) showed optimal diagnostic efficacy (AUC =0.920; sensitivity 85.71%; specificity 89.29%), which was significantly better than that of D (AUC =0.753; Z=2.874; P=0.004), α (AUC =0.715; Z=3.505; P=0.001), K^{trans} (AUC =0.808; Z=2.741; P=0.006), and K_{ep} (AUC =0.832; Z=2.147; P=0.032) alone. There were no statistically significant differences in AUC between any of the individual parameters (*Figure 3*; *Table 5*).

Model validation

Bootstrapping with 1,000 samples was used to validate the multivariate regression model with D and K_{ep} combined. The ROC and calibration curves indicated that the validation model not only had high accuracy in identifying high-proliferation and low-proliferation EC (AUC =0.882; 95% CI: 0.861–0.897; *Figure 4A*), but that it was also highly consistent with the original model (C-statistic 0.902; *Figure 4B*). Moreover, DCA showed that the model could provide a high net benefit for relevant patients (*Figure 4C*).

Correlation analysis

K_{ep} showed a moderate correlation with the Ki-67 index (r=–0.534; P<0.001), K^{trans} and D showed a mild negative

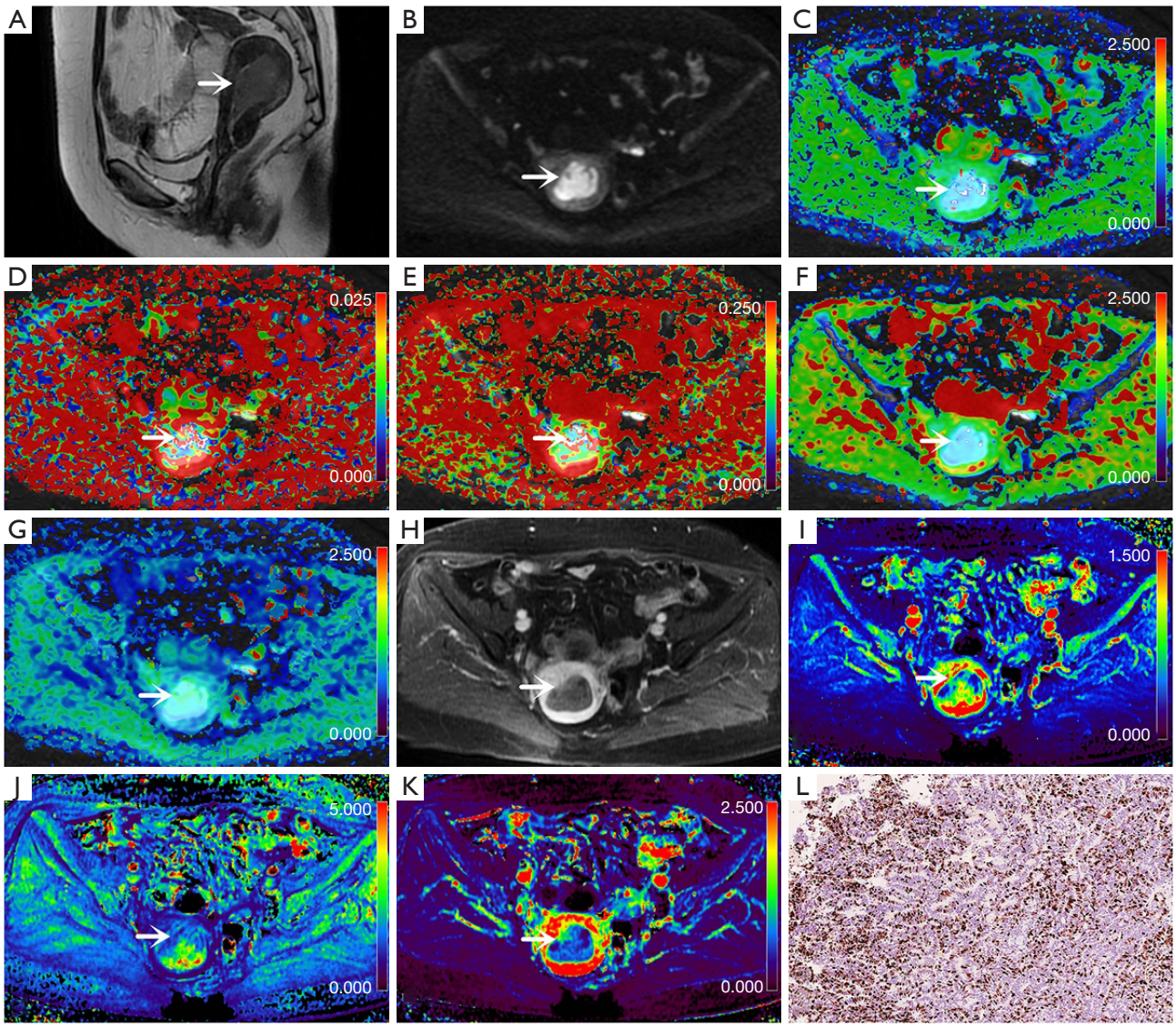

Figure 2 Images from a 57-year-old woman with endometrial carcinoma (arrows; 5 cm × 2.5 cm × 0.8 cm; Ki-67 =40%; grade 2; stage IA). (A) Sagittal T_2-weighted imaging map. (B) Oblique axial diffusion-weighted imaging map (b=800 s/mm^2). (C) Oblique axial colored map of the diffusion coefficient, D. (D) Oblique axial colored map of the pseudo diffusion coefficient, D*. (E) Oblique axial pseudo colored map of the perfusion fraction, f. (F) Oblique axial pseudo colored map of the DDC. (G) Oblique axial colored map of the water molecular diffusion heterogeneity index, α. (H) Oblique axial contrast-enhanced map. (I) Oblique axial colored map of the volume transfer constant, K^{trans}. (J) Oblique axial colored map of the rate transfer constant, K_{ep}. (K) Oblique axial colored map of the volume of extravascular extracellular space per unit volume of tissue, V_e. (L) Immunohistochemical map of Ki-67 staining (Ki-67 =40%; original magnification 200×). D, diffusion coefficient; D*, pseudo diffusion coefficient; f, perfusion fraction; DDC, distributed diffusion coefficient; α, water molecular diffusion heterogeneity index; K^{trans}, volume transfer constant; V_e, volume of extravascular extracellular space per unit volume of tissue; K_{ep}, rate transfer constant.

correlation with the Ki-67 index (K^{trans}: r=–0.409, P<0.001; D: –0.271, P=0.023), and α showed a mild positive correlation with the Ki-67 index (r=0.488; P<0.001). There was no significant correlation between the Ki-67 index and D*, f, DDC, or V_e, with r values of –0.256 (P=0.053), 0.116 (P=0.340), 0.009 (P=0.944), and 0.216 (P=0.072), respectively (*Figure 5*).

Table 2 Clinicopathologic features of patients

Variables	Values
Age (years)	50.17±7.91
Maximum diameter of lesion (mm)	24.55±12.46
FIGO stage	
IA	54 (77.14)
IB	7 (10.00)
II	4 (5.71)
IV	5 (7.14)
Histologic subtype	
Adenocarcinoma	70 (100.00)
Endometrioid carcinoma	68 (97.14)
Serous carcinoma	2 (2.86)
Ki-67 index	
≤10% (–)	10 (14.29)
11–25% (+)	0 (0.00)
26–50% (++)	32 (45.71)
>50% (+++)	28 (40.00)

Data are given as the mean ± SD or n (%). FIGO, International Federation of Gynecology and Obstetrics; SD, standard deviation.

Discussion

Evaluation of DCE-MRI for EC

K^{trans} and K_{ep} are quantitative parameters used in DCE-MRI to reflect the blood supply of tissues. The former represents the rate of contrast agent entering the EES from the blood vessels, whereas the latter reflects the rate of contrast agent returning from the EES to the blood vessels (11). In general, the greater the density and permeability of the microvessels are in the tissue, the greater the values of K^{trans} and K_{ep} (13,14). A few studies have explored the use of K^{trans} and K_{ep} in EC, with results showing that both can be effective in assessing pathophysiological features, such as risk stratification and the histological grade of EC (18,19). In the present study, values of both K^{trans} and K_{ep} were significantly higher in the high-proliferation group than in the low-proliferation group, which is similar to the results reported in the previous studies, indicating the significance of K^{trans} and K_{ep} in the assessment of EC proliferation. Regarding the reason for this result, we speculate that it may be due to the high proliferation and metabolism of EC cells in the high-proliferation group compared with the low-proliferation group, which results in abundant neovascularization and immature vessel walls, accelerating the rate of intra- and extravascular contrast exchange and

Table 3 Comparisons of parameters between the high-proliferation and low-proliferation groups

Parameters	High-proliferation group (n=28)	Low-proliferation group (n=42)	t/Z value	P value
D ($\times10^{-3}$ mm^2/s)	0.83 (0.68–1.20)	0.63 (0.45–0.85)	–3.573	<0.001[a]
D* ($\times10^{-3}$ mm^2/s)	55.60 (30.30–107.50)	38.80 (23.93–93.86)	–1.265	0.206[a]
f (%)	19.50 (14.10–25.40)	19.00 (15.90–30.9)	–0.540	0.590[a]
DDC ($\times10^{-3}$ mm^2/s)	0.91 (0.76–1.52)	0.93 (0.66–1.30)	–1.493	0.136[a]
α	0.79±0.11	0.70±0.13	3.383	0.001[b]
K^{trans} (min^{-1})	0.95 (0.52–1.49)	0.49 (0.20–0.63)	–4.340	<0.001[a]
V_e	0.65±0.20	0.56±0.25	1.557	0.124[b]
K_{ep} (min^{-1})	1.72 (1.12–3.23)	0.82 (0.60–1.22)	–4.687	<0.001[a]

Normally distributed data are presented as the mean ± SD; data that were not normally distributed are presented as the median (interquartile range). [a], independent *t*-test; [b], Mann-Whitney test. D, diffusion coefficient; D*, pseudo diffusion coefficient; f, perfusion fraction; DDC, distributed diffusion coefficient; α, water molecular diffusion heterogeneity index; K^{trans}, volume transfer constant; V_e, volume of extravascular extracellular space per unit volume of tissue; K_{ep}, rate transfer constant; SD, standard deviation.

Table 4 Logistic regression analyses for parameters in identifying high-proliferation and low-proliferation endometrial carcinoma

Parameters	Univariate analyses		Multivariate analyses	
	OR for 1 SD (95% CI)	P value	OR for 1 SD (95% CI)	P value
Age	0.916 (0.854–0.982)	0.014	1.018 (0.923–1.123)	0.724
Tumor size	0.999 (0.961–1.038)	0.948	–	–
FIGO stage	0.585 (0.349–0.981)	0.042	1.214 (0.543–2.714)	0.637
D	4.291 (1.722–10.692)	0.002	16.752 (1.819–154.263)	0.013
D*	1.006 (0.997–1.014)	0.178	–	–
f	0.787 (0.512–1.209)	0.274	–	–
α	0.417 (0.231–0.754)	0.004	0.929 (0.372–2.321)	0.874
DDC	1.629 (0.935–2.836)	0.085	–	–
K^{trans}	18.986 (3.493–103.199)	0.001	13.500 (0.592–307.846)	0.103
V_e	0.202 (0.024–1.709)	0.142	–	–
K_{ep}	16.144 (3.206–81.282)	0.001	14.645 (1.278–167.843)	0.031

All factors with P<0.05 in univariate analyses were included in multivariate regression analyses. FIGO, International Federation of Gynecology and Obstetrics; D, diffusion coefficient; D*, pseudo diffusion coefficient; f, perfusion fraction; α, water molecular diffusion heterogeneity index; DDC, distributed diffusion coefficient; K^{trans}, volume transfer constant; V_e, volume of extravascular extracellular space per unit volume of tissue; K_{ep}, rate transfer constant; OR, odds ratio; SD, standard deviation; CI, confidence interval.

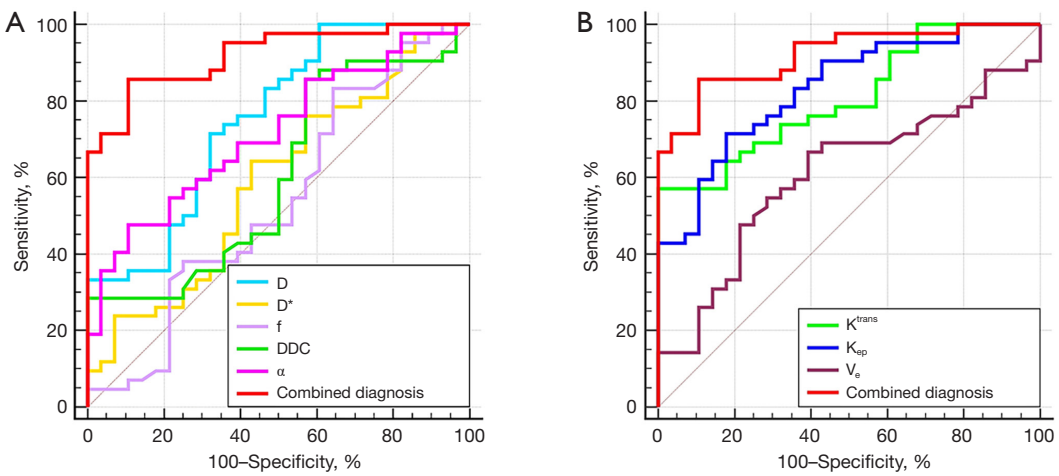

Figure 3 Area under the receiver operating characteristic curves for individual (A) IVIM-derived and (B) dynamic contrast-enhanced magnetic resonance imaging-derived parameters, as well as the combination of independent predictors (D and K_{ep}). D, diffusion coefficient; D*, pseudo diffusion coefficient; f, perfusion fraction; DDC, distributed diffusion coefficient; α, water molecular diffusion heterogeneity index; K_{ep}, rate transfer constant; K^{trans}, volume transfer constant; V_e, volume of extravascular extracellular space per unit volume of tissue; IVIM, intravoxel incoherent motion.

Table 5 Predictive performance for parameters in identifying high-proliferation and low-proliferation endometrial carcinoma

Parameter	AUC (95% CI)	P value	Cutoff	Sensitivity (%)	Specificity (%)	Versus combined diagnosis (D + K_{ep})
D ($\times10^{-3}$ mm^2/s)	0.753 (0.636–0.849)	<0.001	0.695	71.43	67.86	Z=2.874, P=0.004
D* ($\times10^{-3}$ mm^2/s)	0.536 (0.416–0.653)	0.598	–	–	–	–
f (%)	0.538 (0.415–0.658)	0.605	–	–	–	–
α	0.715 (0.595–0.817)	<0.001	0.691	47.62	89.29	Z=3.505, P=0.001
DDC ($\times10^{-3}$ mm^2/s)	0.606 (0.482–0.721)	0.133	–	–	–	–
K^{trans} (min^{-1})	0.808 (0.696–0.892)	<0.001	0.743	57.14	96.43	Z=2.741, P=0.006
V_e	0.607 (0.483–0.721)	0.120	–	–	–	–
K_{ep} (min^{-1})	0.832 (0.724–0.911)	0.204	1.237	71.43	82.14	Z=2.147, P=0.032
Combined diagnosis (D + K_{ep})	0.920 (0.830–0.971)	<0.001	–	85.71	89.29	–

D, diffusion coefficient; D*, pseudo diffusion coefficient; f, perfusion fraction; α, water molecular diffusion heterogeneity index; DDC, distributed diffusion coefficient; K^{trans}, volume transfer constant; V_e, volume of extravascular extracellular space per unit volume of tissue; K_{ep}, rate transfer constant; AUC, area under the receiver operating characteristic curve; CI, confidence interval.

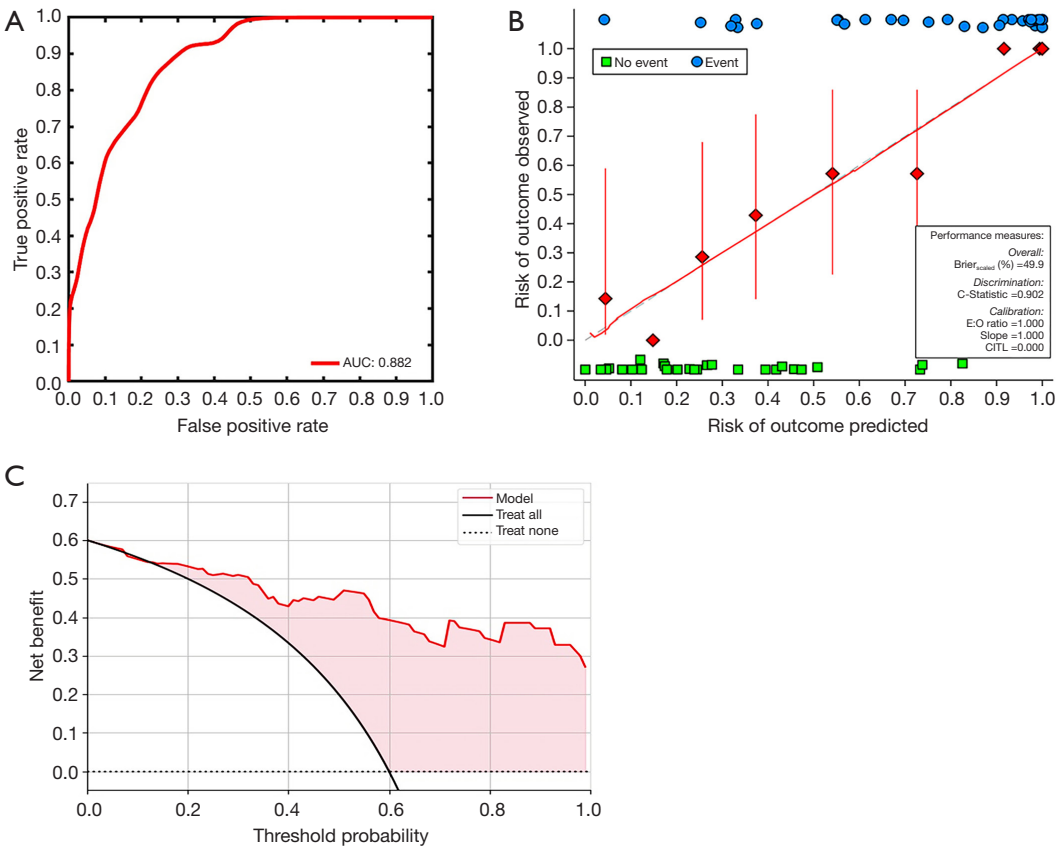

Figure 4 Model validation. (A) AUC, (B) calibration curves, and (C) decision curve analysis for the differentiation of low-proliferation EC from high-proliferation EC in the validation model. AUC, area under the receiver operating characteristic curve; E:O ration, expected:observed ration; CITL, intercept distance; EC, endometrial carcinoma.

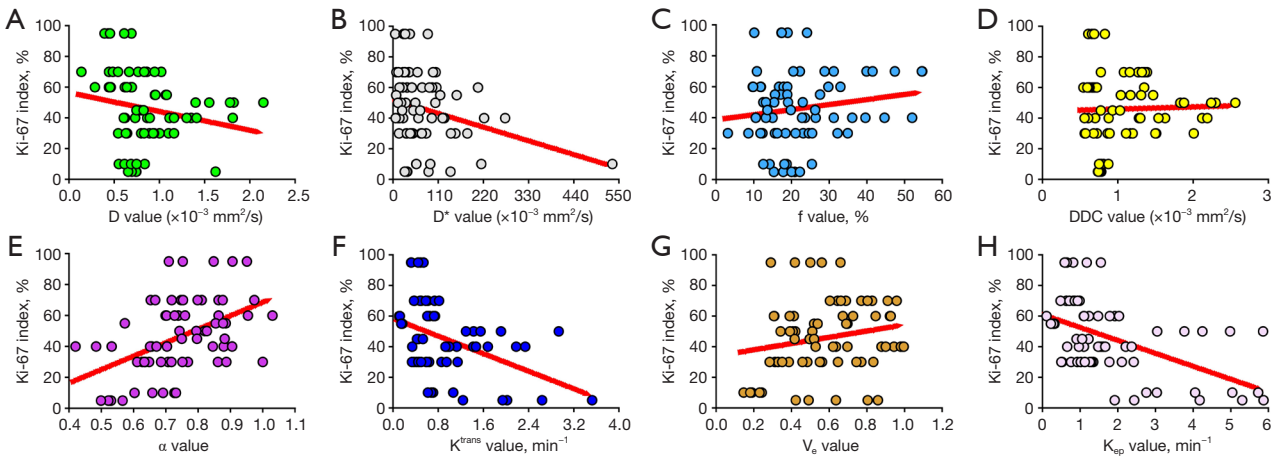

Figure 5 Correlations between the Ki-67 index and (A) the diffusion coefficient, D (r=–0.271; P=0.023), (B) the pseudo diffusion coefficient, D* (r=–0.256; P =0.053), (C) the perfusion fraction, f (r=0.116; P=0.340), (D) the distributed diffusion coefficient (DDC; r=0.009; P=0.944), (E) the water molecular diffusion heterogeneity index, α (r=0.488; P<0.001), (F) the volume transfer constant, K^{trans} (r=–0.409; P <0.001), (G) the volume of extravascular extracellular space per unit volume of tissue, V_e (r=0.216; P =0.072), and (H) the rate transfer constant, K_{ep} (r=–0.534; P<0.001). D, diffusion coefficient; D*, pseudo diffusion coefficient; f, perfusion fraction; DDC, distributed diffusion coefficient; α, water molecular diffusion heterogeneity index; K^{trans}, volume transfer constant; V_e, volume of extravascular extracellular space per unit volume of tissue; K_{ep}, rate transfer constant.

eventually increasing K^{trans} and K_{ep} values (22-24).

V_e is a DCE-MRI parameter that reflects the volume of the EES. Several studies have indicated that the role of V_e in lesion assessment is not ideal due to its poor stability and vulnerability to factors such as lesion edema and microcystic changes (18,25,26). In the present study, there was no statistically significant difference in V_e between the high-proliferation and low-proliferation groups, which is similar to previously reported results, indicating that V_e cannot distinguish EC under different proliferation conditions. However, there have been contradictory reports. For example, the study of Satta *et al.* concluded that EC with higher histological grade had increased EES and larger V_e values due to a greater degree of necrosis (19), and Koo *et al.* suggested that breast lesions with higher malignancy tend to have lower EES and reduced V_e due to faster proliferation and a tighter cell structure (27). These inconsistent findings may be due to the use of different methods to quantify perfusion parameters and differences between study participants. In the future, we will refine the relevant studies to further explore the role of V_e in EC assessment.

Gadolinium contrast agent is the basis of DCE-MRI examinations. It can be injected intravenously to highlight the lesions, so it is widely used in the diagnosis and evaluation of various diseases. In the present study, DCE-MRI based on GD-DTPA showed good results in predicting the proliferation status of patients with EC, which further demonstrated the value of gadolinium contrast agent in disease diagnosis. However, studies have shown that gadolinium contrast agent can be deposited in multiple organs in the body, and its distribution and deposition in the body are closely related to the type of gadolinium contrast agent and intravenous dose (28,29). Therefore, future studies should explore the mechanism of gadolinium contrast agent deposition, possible adverse reactions, and the principle of its safe administration as important topics related to the further application of DCE-MRI.

Evaluation of IVIM for EC

D is one of the quantitative parameters of biexponential model IVIM and theoretically reflects the diffusion movement of water molecules in the tissue more realistically because the effect of microcirculatory perfusion is excluded (9,10). Previous studies have shown that lesions with higher Ki-67 expression have higher cell densities, tend to have more significant water molecule restriction, and have smaller D values (30,31). In the present study, D was

significantly lower in the high-proliferation group than in the low-proliferation group and was one of the independent predictors for the discrimination between the two groups, which is consistent with the findings of previous studies and suggests that D value has a positive significance in the prediction of Ki-67 status in EC. However, in a study of 54 patients with EC, Li *et al.* reported no significant difference in D values between the high-proliferation (Ki-67 >30%) and low-proliferation (Ki-67 ≤30%) groups (32). We suggest that the different scanning parameters of IVIM sequences and the differences in Ki-67 values used to define the high-proliferation and low-proliferation groups might have contributed to the apparent discrepancy.

DDC is the parameter used by the stretched exponential model IVIM to reflect the diffusion movement status of water molecules in tissues; some studies have shown that DDC facilitates the noninvasive assessment of proliferation status in glioma and lung cancer (29,33). However, to the best of our knowledge, no authoritative investigations have reported the value of DDC in assessing the Ki-67 proliferation status in EC. In the present study, there was no significant difference in DDC between the high-proliferation and low-proliferation EC groups, which is not consistent with the findings of the previous studies related to glioma (33) and lung cancer (31). We speculate that this may be related to the fact that there are more factors within high-proliferation EC that promote the diffusion movement of water molecules, such as a richer blood supply and more necrotic components, and that DDC is unable to separate these factors as effectively as D does (9,34,35). In addition, differences in microstructure among EC, glioma, and lung cancer might have contributed to the variation in the diagnostic efficacy of DDC among studies.

D* and f are the parameters used by the biexponential model IVIM to reflect microcirculatory perfusion information, and these are dissimilar to the DCE-MRI perfusion parameters, whose magnitude is primarily related to factors such as intra-tissue microvascular density and intra-microvascular blood flow rate (9,10). Previous studies have shown that although high-proliferation lesions are metabolically active and rich in neovascularization, because of the tight tissue structure, tortuous vascularity, and the presence of more necrotic tissue, the overall internal vascular density and blood flow velocity in the microcirculation do not change significantly compared with those of low-proliferation lesions, so it is difficult to effectively differentiate high-proliferation and low-proliferation lesions using D* and f (15,31,32). In the present study, the differences in D* and f between the high-proliferation and low-proliferation groups of EC were not significant, which is consistent with the findings of the abovementioned studies and demonstrates the difficulty of using D* and f for the reliable assessment of EC proliferation. However, considering the close connection between D* and f and the choice of b value during IVIM sequence scanning (36,37), we will explore the role of these two parameters in the evaluation of EC proliferation under different b value settings in future studies.

The stretched exponential model IVIM generates α, a parameter reflecting the complexity of the tissue. Previous studies have found that due to the higher level of intravoxel microscopic necrotic foci, heterogeneous cellularity, and heterogeneous cellularity, the tissue complexity of high-proliferation lesions tends to be higher than that of low-proliferation lesions, and therefore α tends to decrease in high-proliferation lesions (38,39). These results are consistent with those of the present study, suggesting that α can play an important role in the assessment of EC proliferation.

Although some of the IVIM parameters in this study played an important role in the assessment of proliferation status in EC, the IVIM technique itself still suffers from certain shortcomings. In examples of acute brain ischemia MRI and liver, a reduction of perfusion was found to cause artificial elevation of the slow diffusion measure (40,41). A high noise level can flatten the signal decay curve, particularly at high b values, and lead to a reduction in D, which in turn results in an artificially higher f and D*. In the present study, this inevitable noise might have also contributed to an artificially high D* and f, leading to insensitive results. Therefore, we speculate that the combination of IVIM with other techniques may provide stronger measurements, as in this study with DCE-MRI.

This study has several limitations. First, the MRI system used in the study was 1.5 T, and the imaging quality and parameter reliability of DCE-MRI and IVIM sequences may be slightly inferior compared with those of 3.0-T MRI. Second, our study was performed at a single institution with a relatively small number of patients, which might have led to selection bias. Third, the present study avoided areas of cystic degeneration, necrosis, apparent signs and hemorrhage artifacts, or vessels in delineating the ROI, which might have affected the estimation of several parameters. Fourth, unlike in breast cancer, in EC there are no guidelines standardizing the classification of high-proliferation and low-proliferation lesions (2). In this study,

we classified the strongly positive lesions (Ki-67, +++; >50%) as the high-proliferation group and slightly positive (Ki-67, +; <10%) and positive (Ki-67, ++; 10–50%) lesions as the low-proliferation group based on immunohistochemical results and clinical routine, which might have had some effect on the final results.

Conclusions

In conclusion, biexponential model IVIM-, stretched exponential model IVIM-, and DCE-MRI-derived quantitative parameters, including D, α, K^{trans}, and K_{ep}, were significantly associated with Ki-67 status in patients with EC, and the combination of D and K^{trans} may serve as a superior imaging marker for the identification of low-proliferation and high-proliferation ECs.

Acknowledgments

Funding: This work was supported by the Roentgen Imaging Research Project (No. HN-20201017-002) and the Key Project of Henan Province Medical Science and Technology Project (Nos. LHGJ20200519 and 2018020367).

Footnote

Reporting Checklist: The authors have completed the STARD reporting checklist. Available at https://qims.amegroups.com/article/view/10.21037/qims-22-688/rc

Conflicts of Interest: All authors have completed the ICMJE uniform disclosure form (available at https://qims.amegroups.com/article/view/10.21037/qims-22-688/coif). KW and JG report that they are employees of GE Healthcare and were MR collaborating scientists providing technical support under the GE collaboration regulations, but have no financial or other conflicts with respect to this study. The other authors have no conflicts of interest to declare.

Ethical Statement: The authors are accountable for all aspects of the work in ensuring that questions related to the accuracy or integrity of any part of the work are appropriately investigated and resolved. The study was conducted in accordance with the Declaration of Helsinki (as revised in 2013). This prospective study complied with ethical committee standards and was approved by the Ethics Committee of the First Affiliated Hospital of Xinxiang Medical University (No. EC-022-002); informed consent was obtained from all participants.

References

1. Siegel RL, Miller KD, Fuchs HE, Jemal A. Cancer Statistics, 2021. CA Cancer J Clin 2021;71:7-33.
2. Kitson S, Sivalingam VN, Bolton J, McVey R, Nickkho-Amiry M, Powell ME, Leary A, Nijman HW, Nout RA, Bosse T, Renehan AG, Kitchener HC, Edmondson RJ, Crosbie EJ. Ki-67 in endometrial cancer: scoring optimization and prognostic relevance for window studies. Mod Pathol 2017;30:459-68.
3. Ocak B, Atalay FÖ, Sahin AB, Ozsen M, Dakiki B, Türe S, Mesohorli M, Odman HU, Tanrıverdi Ö, Ocakoğlu G, Bayrak M, Ozan H, Demiröz C, Sali S, Orhan SO, Deligönül A, Cubukcu E, Evrensel T. The impact of Ki-67 index, squamous differentiation, and several clinicopathologic parameters on the recurrence of low and intermediate-risk endometrial cancer. Bosn J Basic Med Sci 2021;21:549-54.
4. Visser NCM, Reijnen C, Massuger LFAG, Nagtegaal ID, Bulten J, Pijnenborg JMA. Accuracy of Endometrial Sampling in Endometrial Carcinoma: A Systematic Review and Meta-analysis. Obstet Gynecol 2017;130:803-13.
5. Garcia TS, Appel M, Rivero R, Kliemann L, Wender MC. Agreement Between Preoperative Endometrial Sampling and Surgical Specimen Findings in Endometrial Carcinoma. Int J Gynecol Cancer 2017;27:473-8.
6. Aracki-Trenkic A, Stojanov D, Petric A, Benedeto-Stojanov D, Trenkic M, Ignjatovic J. The role of magnetic resonance imaging in the evaluation of endometrial carcinoma. J BUON 2016;21:542-8.
7. Cashmore MT, McCann AJ, Wastling SJ, McGrath C, Thornton J, Hall MG. Clinical quantitative MRI and the need for metrology. Br J Radiol 2021;94:20201215.
8. Curtis WA, Fraum TJ, An H, Chen Y, Shetty AS, Fowler KJ. Quantitative MRI of Diffuse Liver Disease:

Current Applications and Future Directions. Radiology 2019;290:23-30.
9. Iima M. Perfusion-driven Intravoxel Incoherent Motion (IVIM) MRI in Oncology: Applications, Challenges, and Future Trends. Magn Reson Med Sci 2021;20:125-38.
10. Iima M, Le Bihan D. Clinical Intravoxel Incoherent Motion and Diffusion MR Imaging: Past, Present, and Future. Radiology 2016;278:13-32.
11. Khalifa F, Soliman A, El-Baz A, Abou El-Ghar M, El-Diasty T, Gimel'farb G, Ouseph R, Dwyer AC. Models and methods for analyzing DCE-MRI: a review. Med Phys 2014;41:124301.
12. Noij DP, Martens RM, Marcus JT, de Bree R, Leemans CR, Castelijns JA, de Jong MC, de Graaf P. Intravoxel incoherent motion magnetic resonance imaging in head and neck cancer: A systematic review of the diagnostic and prognostic value. Oral Oncol 2017;68:81-91.
13. Meyer HJ, Höhn AK, Surov A. Associations between dynamic-contrast enhanced MRI and tumor infiltrating lymphocytes and tumor-stroma ratio in head and neck squamous cell cancer. Cancer Imaging 2021;21:60.
14. Kang SR, Kim HW, Kim HS. Evaluating the Relationship Between Dynamic Contrast-Enhanced MRI (DCE-MRI) Parameters and Pathological Characteristics in Breast Cancer. J Magn Reson Imaging 2020;52:1360-73.
15. Meng N, Wang XJ, Sun J, Huang L, Wang Z, Wang KY, Wang J, Han DM, Wang MY. Comparative Study of Amide Proton Transfer-Weighted Imaging and Intravoxel Incoherent Motion Imaging in Breast Cancer Diagnosis and Evaluation. J Magn Reson Imaging 2020;52:1175-86.
16. Lee S, Choi YH, Cho YJ, Cheon JE, Moon JS, Kang GH, Kim WS. Quantitative evaluation of Crohn's disease using dynamic contrast-enhanced MRI in children and young adults. Eur Radiol 2020;30:3168-77.
17. Meng N, Fang T, Feng P, Huang Z, Sun J, Wang X, Shang J, Wang K, Han D, Wang M. Amide Proton Transfer-Weighted Imaging and Multiple Models Diffusion-Weighted Imaging Facilitates Preoperative Risk Stratification of Early-Stage Endometrial Carcinoma. J Magn Reson Imaging 2021;54:1200-11.
18. Ye Z, Ning G, Li X, Koh TS, Chen H, Bai W, Qu H. Endometrial carcinoma: use of tracer kinetic modeling of dynamic contrast-enhanced MRI for preoperative risk assessment. Cancer Imaging 2022;22:14.
19. Satta S, Dolciami M, Celli V, Di Stadio F, Perniola G, Palaia I, Pernazza A, Della Rocca C, Rizzo S, Catalano C, Capuani S, Manganaro L. Quantitative diffusion and perfusion MRI in the evaluation of endometrial cancer: validation with histopathological parameters. Br J Radiol 2021;94:20210054.
20. Shieh G. Choosing the best index for the average score intraclass correlation coefficient. Behav Res Methods 2016;48:994-1003.
21. Xu C, Yu Y, Li X, Sun H. Value of integrated PET-IVIM MRI in predicting lymphovascular space invasion in cervical cancer without lymphatic metastasis. Eur J Nucl Med Mol Imaging 2021;48:2990-3000.
22. Shin JK, Kim JY. Dynamic contrast-enhanced and diffusion-weighted MRI of estrogen receptor-positive invasive breast cancers: Associations between quantitative MR parameters and Ki-67 proliferation status. J Magn Reson Imaging 2017;45:94-102.
23. Nunobiki O, Taniguchi E, Ishii A, Tang W, Utsunomiya H, Nakamura Y, Mori I, Kakudo K. Significance of hormone receptor status and tumor vessels in normal, hyperplastic and neoplastic endometrium. Pathol Int 2003;53:846-52.
24. Chen J, Chen C, Xia C, Huang Z, Zuo P, Stemmer A, Song B. Quantitative free-breathing dynamic contrast-enhanced MRI in hepatocellular carcinoma using gadoxetic acid: correlations with Ki67 proliferation status, histological grades, and microvascular density. Abdom Radiol (NY) 2018;43:1393-403.
25. Liu C, Wang K, Chan Q, Liu Z, Zhang J, He H, Zhang S, Liang C. Intravoxel incoherent motion MR imaging for breast lesions: comparison and correlation with pharmacokinetic evaluation from dynamic contrast-enhanced MR imaging. Eur Radiol 2016;26:3888-98.
26. Cho N, Im SA, Park IA, Lee KH, Li M, Han W, Noh DY, Moon WK. Breast cancer: early prediction of response to neoadjuvant chemotherapy using parametric response maps for MR imaging. Radiology 2014;272:385-96.
27. Koo HR, Cho N, Song IC, Kim H, Chang JM, Yi A, Yun BL, Moon WK. Correlation of perfusion parameters on dynamic contrast-enhanced MRI with prognostic factors and subtypes of breast cancers. J Magn Reson Imaging 2012;36:145-51.
28. Kanda T, Ishii K, Kawaguchi H, Kitajima K, Takenaka D. High signal intensity in the dentate nucleus and globus pallidus on unenhanced T1-weighted MR images: relationship with increasing cumulative dose of a gadolinium-based contrast material. Radiology 2014;270:834-41.
29. Sanyal S, Marckmann P, Scherer S, Abraham JL. Multiorgan gadolinium (Gd) deposition and fibrosis in a patient with nephrogenic systemic fibrosis--an autopsy-based review. Nephrol Dial Transplant 2011;26:3616-26.

30. Xiao Z, Zhong Y, Tang Z, Qiang J, Qian W, Wang R, Wang J, Wu L, Tang W, Zhang Z. Standard diffusion-weighted, diffusion kurtosis and intravoxel incoherent motion MR imaging of sinonasal malignancies: correlations with Ki-67 proliferation status. Eur Radiol 2018;28:2923-33.
31. Huang Z, Li X, Wang Z, Meng N, Fu F, Han H, Li D, Bai Y, Wei W, Fang T, Feng P, Yuan J, Yang Y, Wang M. Application of Simultaneous (18) F-FDG PET With Monoexponential, Biexponential, and Stretched Exponential Model-Based Diffusion-Weighted MR Imaging in Assessing the Proliferation Status of Lung Adenocarcinoma. J Magn Reson Imaging 2022;56:63-74.
32. Li Y, Lin CY, Qi YF, Wang X, Chen B, Zhou HL, Ren J, Yang JJ, Xiang Y, He YL, Xue HD, Jin ZY. Three-dimensional turbo-spin-echo amide proton transfer-weighted and intravoxel incoherent motion MR imaging for type I endometrial carcinoma: Correlation with Ki-67 proliferation status. Magn Reson Imaging 2021;78:18-24.
33. Chaudhary N, Zhang G, Li S, Zhu W. Monoexponential, biexponential and stretched exponential models of diffusion weighted magnetic resonance imaging in glioma in relation to histopathologic grade and Ki-67 labeling index using high B values. Am J Transl Res 2021;13:12480-94.
34. Kim SY, Kim EK, Moon HJ, Yoon JH, Koo JS, Kim SG, Kim MJ. Association among T2 signal intensity, necrosis, ADC and Ki-67 in estrogen receptor-positive and HER2-negative invasive ductal carcinoma. Magn Reson Imaging 2018;54:176-82.
35. Chen Y, Qin X, Long L, Zhang L, Huang Z, Jiang Z, Li C. Diagnostic Value of Gd-EOB-DTPA-Enhanced MRI for the Expression of Ki67 and Microvascular Density in Hepatocellular Carcinoma. J Magn Reson Imaging 2020;51:1755-63.
36. Pang Y, Turkbey B, Bernardo M, Kruecker J, Kadoury S, Merino MJ, Wood BJ, Pinto PA, Choyke PL. Intravoxel incoherent motion MR imaging for prostate cancer: an evaluation of perfusion fraction and diffusion coefficient derived from different b-value combinations. Magn Reson Med 2013;69:553-62.
37. Wang YXJ, Huang H, Zheng CJ, Xiao BH, Chevallier O, Wang W. Diffusion-weighted MRI of the liver: challenges and some solutions for the quantification of apparent diffusion coefficient and intravoxel incoherent motion. Am J Nucl Med Mol Imaging 2021;11:107-42.
38. Zhang J, Chen X, Chen D, Wang Z, Li S, Zhu W. Grading and proliferation assessment of diffuse astrocytic tumors with monoexponential, biexponential, and stretched-exponential diffusion-weighted imaging and diffusion kurtosis imaging. Eur J Radiol 2018;109:188-95.
39. Fu F, Meng N, Huang Z, Sun J, Wang X, Shang J, Fang T, Feng P, Wang K, Han D, Wang M. Identification of histological features of endometrioid adenocarcinoma based on amide proton transfer-weighted imaging and multimodel diffusion-weighted imaging. Quant Imaging Med Surg 2022;12:1311-23.
40. Wáng YXJ. Mutual constraining of slow component and fast component measures: some observations in liver IVIM imaging. Quant Imaging Med Surg 2021;11:2879-87.
41. Wáng YXJ. A reduction of perfusion can lead to an artificial elevation of slow diffusion measure: examples in acute brain ischemia MRI intravoxel incoherent motion studies. Ann Transl Med 2021;9:895.

Cite this article as: Zhang G, Yan R, Liu W, Jin X, Wang X, Wang H, Li Z, Shang J, Wang K, Guo J, Han D. Use of biexponential and stretched exponential models of intravoxel incoherent motion and dynamic contrast-enhanced magnetic resonance imaging to assess the proliferation of endometrial carcinoma. Quant Imaging Med Surg 2023;13(4):2568-2581. doi: 10.21037/qims-22-688

